Amorphous and Nanocrystalline Anatase Titanium Dioxide Prepared from Peroxo-Polytitanic Acid and Their Electrochemical Properties

Isao Tsuyumoto, and Kazuki Kobayashi

Department of Applied Chemistry, College of Bioscience and Chemisrty,
Kanazawa Institute of Technology, Nonoichi, Ishikawa 9218501, JAPAN

Peroxo-polytitanic acid solution was obtained by a reaction between metallic Ti powder and 30 wt% aq. H_2O_2. Amorphous titanium dioxide was obtained as dried residue at 115 °C, and nanocrystalline anatase titanium dioxide was obtained by heating the amorphous phase at 300 – 500 °C. The anatase titanium dioxide with average particle size of 25 nm obtained by heating at 300 °C for 5h showed the capacity of 158 mAh/g as negative electrode for lithium ion batteries. The capacity was increased with increasing the heating time at 300 °C. Lattice defects were reduced by heating at 300 °C without crystal growth and aggregation, and this enhanced the lithium insertion/deinsertion performance. We also calculated site energy distribution from the deconvolution of experimental discharge curves, and discussed the relationship between the structure and the insertion site.

Introduction

Titanium dioxides, such as anatase, rutile, hollandite, TiO_2 (B), have been intensively investigated as negative electrode materials for lithium ion batteries (1-9). Among them, anatase forms showed lithium insertion/deinsertion performance depending on the preparation method and the resultant morphology. Small particle size compatible with few lattice defects is favorable for the diffusion efficiency of lithium ion into and out of particles, and such new preparation method is highly desirable to achieve good lithium insertion/deinsertion performance. We have developed a new method for preparing titanium-containing aqueous solutions using a reaction between metallic titanium powder and 30 – 70 wt% aq. H_2O_2 (10). The yield solution is peroxo-polytitanic acid (titanium isopolyacid, Ti-IPA), and the precipitates from the Ti-IPA solution are used as precursors for not only titanium oxides but also titanium complex oxides such as $BaTiO_3$.

In the present study, we investigated lithium insertion/deinsertion properties of amorphous and nanocrystalline anatase titanium dioxides prepared by the new method using Ti-IPA solutions. Furthermore, we also calculated the site energy distribution from the experimental charge/discharge curves using a numerical deconvolution technique, because the charge/discharge curves are the function of the energy distribution of lithium insertion site in host materials.

Experimental

Sample Preparation

Metallic titanium powder (0.36 g, 45 μm particle size) was dispersed in 150 mL of 30 wt % aq. H_2O_2 solution at room temperature, and the dissolving reaction proceeded mildly with the emission of oxygen gas. A yellow transparent solution of peroxo-polytitanic acid (Ti-IPA) was obtained in 24 h. After removing insolubles, Ti-IPA solution was dried at 115 °C for 24h to yield yellow powder. The yellow powder was amorphous TiO_2. By heating the amorphous TiO_2 at 300 – 500 °C in air, we obtained anatase TiO_2.

Characterization

The powder XRD patterns of the products were measured with a diffractometer using graphite monochromatized Cu *K*α radiation (λ= 0.15406 nm). The crystalline parameters of the anatase forms were refined by the Rietveld method using the RIETAN-FP (11). The crystallite sizes were determined by the Scherrer equation. Each sample of 16.6 – 16.7 mg was intimately ground with acetylene black (AB) at weight ratio of 1:1. The TiO_2/AB composite was mixed with polytetrafluoroethylene (PTFE) binder and pressed onto a copper mesh for the lithium insertion/deinsertion measurements. The Ag/Ag^+ electrode for non-aqueous solvent (RE-7, ALS Corporation Ltd., Tokyo, Japan) was used as a reference electrode, and $LiCoO_2$ with AB and PTFE as a counter electrode. A 1 M $LiClO_4$ ethylene carbonate (EC) / diethyl carbonate (DEC) solution (EC:DEC=1:1 in volume) was used as an electrolyte. The measurements were carried out in the galvanostatic mode at 3.0 mA (1.08 C) in the range 1.0 – 3.5 V (vs Li).

Results and Discussion

Crystal Structure and Lithium Insertion/Deinsertion Properties

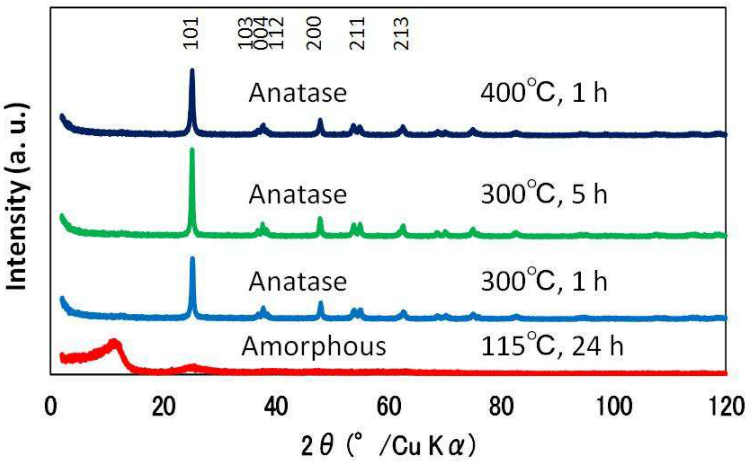

Figure 1. Powder XRD patterns of titanium oxides prepared from Ti-IPA (peroxo-polytitanic acid). Amorphous phase is the residue of Ti-IPA aq dried at 115 °C for 24 h, and nanocrystalline anatase forms are obtained by heating the amorphous phase.

TABLE I. Structural Parameters refined by the Rietveld Method and Crystallite Sizes. Tetragonal, Space Group; $I\,4_1$ / amd (144). All occupancies are fixed at unity.

Heating Condition	Lattice Parameter	Site Coordinate and Atomic position	Crystallite Size
300 °C, 1 h	*a*=3.789, *c*=9.512	Ti 4*a* (0, 3/4, 1/8) O 8*e* (0, 1/4, *u*), *u*=0.208	22 nm
300 °C, 5 h	*a*=3.796, *c*=9.527	Ti 4*a* (0, 3/4, 1/8) O 8*e* (0, 1/4, *u*), *u*=0.206	25 nm
400 °C, 1 h	*a*=3.793, *c*=9.521	Ti 4*a* (0, 3/4, 1/8) O 8*e* (0, 1/4, *u*), *u*=0.207	22 nm
400 °C, 5 h	*a*=3.787, *c*=9.512	Ti 4*a* (0, 3/4, 1/8) O 8*e* (0, 1/4, *u*), *u*=0.205	26 nm
500 °C, 1 h	*a*=3.786, *c*=9.515	Ti 4*a* (0, 3/4, 1/8) O 8*e* (0, 1/4, *u*), *u*=0.208	25 nm
500 °C, 5 h	*a*=3.790, *c*=9.524	Ti 4*a* (0, 3/4, 1/8) O 8*e* (0, 1/4, *u*), *u*=0.207	27 nm

Figure 1 shows the XRD patterns of amorphous TiO_2 obtained as the residue of Ti-IPA solution dried at 115 °C for 24 h and of nanocrystalline anatase TiO_2 obtained by heating the amorphous TiO_2 at 300 or 400 °C. Table I shows structural parameters refined by the Rietveld method and crystallite sizes. The space group, $I\,4_1$/amd, and the site cooridinates were the same as that of the conventional anatase TiO_2 (12,13). The amorphous phase crystallized into the anatase form over around 300 °C. By the extension of heating time from 1 h to 5 h at 300 °C, the lattice parameter *c* was increased from 0.9512 nm to 0.9527 nm, and the former parameter was close to the conventional anatase form. The crystallite sizes of heating time 1 h and 5 h at 300 °C were 22 nm and 25 nm, respectively, indicating that crystal growth hardly proceeds around 300 °C.

The amorphous TiO_2 showed steep potential changes without plateau regions upon lithium insertion and deinsertion as shown in Figure 2 (a). The capacity was about 60 mAh/g much lower than the theoretical value 168 mAh/g. This indicates that the lithium insertion sites in the amorphous phase are heterogeneous and more than half of them are unsuitable for lithium insertion due to spatial or energetic reason. Figures 2 (b), (c) and (d) show charge/discharge curves of nanocrystalline anatase TiO_2 obtained by heating at 300 °C for 1 h, at 300 °C for 5 h, and at 400 °C for 1 h, respectively. A plateau region was observed in each charge/discharge curve, indicating homogeneous lithium insertion sites. The capacity was increased from 109 mAh/g to 158 mAh/g with increasing the heating time from 1 h to 5 h. The capacity 158 mAh/g close to the theoretical value was achieved at rather high rate 1.08 C using the nanocrystalline anatase TiO_2 obtained at 300 °C for 5 h. Additionally, as shown in Figures 2 (e) and (f), the capacities of the anatase TiO_2 obtained at 400 °C and 500 °C for 5 h were 143 mAh/g and 121 mAh/g, respectively. Elevating the heating temperature resulted in the reduction of the capacity, because crystal growth and aggregation to form secondary particles at elevating temperatures are not favorable for the diffusion of lithium ion into and out of the particles. We can say that heating the amorphous precursor at 300 °C is the most appropriate route to prepare nanocrystalline anatase TiO_2 for lithium insertion and deinsertion, because crystal growth and aggregation are suppressed and lattice defects are reduced at 300 °C.

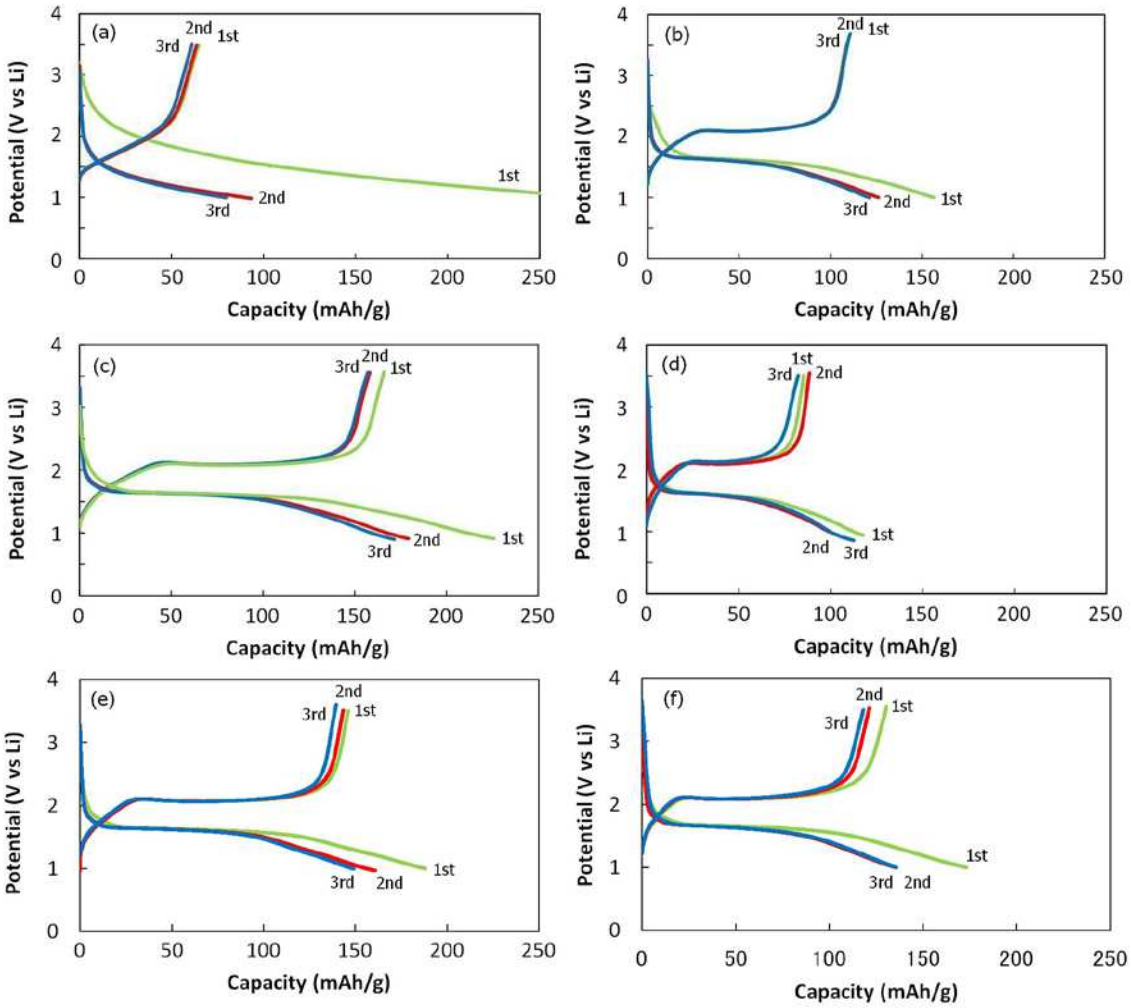

Figure 2. Charge/discharge curves of the titanium oxides prepared from Ti-IPA by heat treatment of (a) 115 °C, 24 h; (b) 300 °C, 1 h; (c) 300 °C, 5 h; (d) 400 °C, 1 h; (e) 400 °C, 5h; and (f) 500 °C, 5 h.

Theoretical Relationship between Site Energy Distribution and OCV Curves

The electrode potential E (vs. Li) of lithium insertion materials is determined by the chemical potential difference between the inserted Li in host electrode $\mu_{\text{Li, host}}$ and the Li metal electrode $\mu_{\text{Li, metal}}$. When we set the chemical potential of the Li metal electrode $\mu_{\text{Li, metal}}$ at zero, and consider the electrode potential E and the chemical potential of the inserted Li $\mu_{\text{Li, host}}$ as a function of Li content x in host electrode, the electrode potential is

$$E(x) = -\frac{\mu_{Li,host}(x)}{F}, \qquad [1]$$

where F is the Faraday constant. Thus, the theoretical OCV (open circuit voltage) curves are derived by the calculation of the chemical potential of Li in host electrode as a function of Li content x.

If the host material has insertion sites with homogeneous site energy ε (< 0) and total number N, and n sites among N are occupied by inserted Li, the internal energy change by the insertion is

$$\triangle U = n\varepsilon, \qquad [2]$$

and the entropy change by the insertion is

$$\triangle S = k \ln \frac{N!}{n!(N-n)!}, \qquad [3]$$

where k is the Boltzmann constant. In the present case, $\triangle H$ is considered to be equal to $\triangle U$, because the volume change is negligibly small. The Gibbs energy change is

$$\triangle G = n\varepsilon - kT \ln \frac{N!}{n!(N-n)!}. \qquad [4]$$

The chemical potential $\mu_{\text{Li, host}}$ is obtained by differentiating Eq. 4 with respect to n

$$\mu_{\text{Li, host}}(x) = \varepsilon + kT \ln \frac{x}{1-x}, \qquad [5]$$

where $x = n/N$ (14). This equation bears close analogy to the Langmuir adsorption isotherm.

Let us consider a host material whose site energy has a wide distribution. In case of amorphous host materials, innumerable kinds of insertion sites exist and each site energy is different from the other kinds of sites in varying degrees. The inserted Li is distributed among the sites so that the chemical potential of Li in each site becomes equal to each other.

If we denote each site energy by ε_1, ε_2, ε_3, $\cdots$ and the occupancy of each site by f_1, f_2, f_3, $\cdots$, the chemical potential of Li in each site is equally given by

$$\begin{aligned} \mu &= \varepsilon_1 + kT \ln \frac{f_1}{1-f_1} \\ &= \varepsilon_2 + kT \ln \frac{f_2}{1-f_2} \\ &= \varepsilon_3 + kT \ln \frac{f_3}{1-f_3} \\ &\cdots \end{aligned} \qquad [6]$$

.

By transforming Eq. 6, we obtain

$$f_i = \frac{1}{1+exp\left(-\frac{\mu-\varepsilon_i}{kT}\right)} \quad (i = 1, 2, 3, \cdots). \qquad [7]$$

This equation indicates that the inserted Li obeys the Fermi distribution function in each site. If we denote the number of each site by N_1, N_2, N_3, $\cdots$, the number of each occupied site by n_1, n_2, n_3, $\cdots$, and the total number of the occupied sites by n, we obtain

$$n = \Sigma \frac{N_i}{1+exp\left(-\frac{\mu-\varepsilon_i}{kT}\right)} \quad (i = 1, 2, 3, \cdots). \qquad [8]$$

If we define a density function $g(\varepsilon) = dN(\varepsilon) / d\varepsilon$ by assuming N_i shows a continuous distribution as a function of ε_i, Eq. 8 gives

$$n = \int_{-\infty}^{\infty} \frac{g(\varepsilon)}{1+exp\left(-\frac{\mu-\varepsilon}{kT}\right)} d\varepsilon \quad . \qquad [9]$$

Eq. 9 is a theoretical derivation of OCV curves, because the capacity corresponds to n and the potential to $-\mu/e$. It is interesting to note that the capacity is a convolution of the density function $g(\varepsilon)$ and the fermi function

$$f(x) = \frac{1}{1+exp\left(-\frac{x}{kT}\right)} \ , \qquad [10]$$

as

$$n(\mu) = \int_{-\infty}^{\infty} f(\mu-\varepsilon) g(\varepsilon) d\varepsilon \quad . \qquad [11]$$

Thus, we can calculate the density function $g(\varepsilon)$ from the OCV curve using a deconvolution method. In dataprocessing, when $n(\mu)$ and $g(\varepsilon)$ are the datasets consisting of m values, we denote $n(\mu)$ and $g(\varepsilon)$ by $(m \times 1)$ matrices and $f(x)$ by $(m \times m)$ matrix. Because the dataset of $n(\mu)$ is the product of matrices denoting $f(x)$ and $g(\varepsilon)$, we obtain the dataset of $g(\varepsilon)$ by multiplying an inverse matrix of $f(x)$ with the dataset of $n(\mu)$. We calculated the inverse matrix of $f(x)$ by the Gauss - Seidel method so as to yield the dataset of $g(\varepsilon)$.

Energy Distribution Curve of Lithium Insertion Sites Calculated from Discharge Curve

Figure 3 shows energy distribution curves of lithium insertion sites calculated from the discharge curves using Eq. 11. The abscissa is proportional to the number of insertion sites and the peak area is proportional to the total number of insertion sites. The nanocrystalline anatase TiO_2 had uniform site energy distributions around 2.1 V, indicating that the insertion sites are homogeneous in the nanocrystalline anatase form. On the other hand, the amorphous phase had a broad energy distribution from 1.3 V to 3.5 V peaking at about 1.6 V. Our results indicate that the amorphous phase has a disadvantage in lithium insertion and deinsertion, because the insertion sites are energetically and spatially heterogeneous. Here we demonstrate that energy distribution curves are numerically calculated from discharge curves and very useful to discuss the relationship between crystal structures and discharge properties.

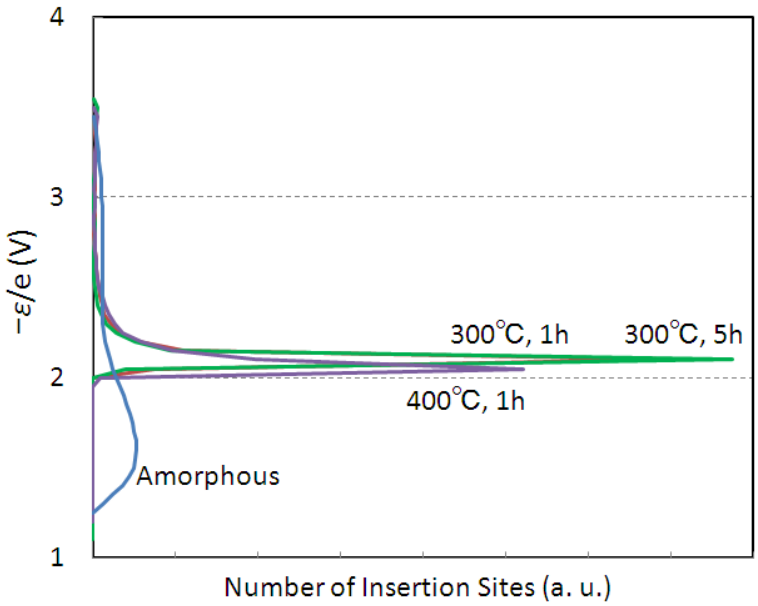

Figure 3. Energy distribution curves of lithium insertion sites calculated by the numerical deconvolution of the discharge curves.

Conclusions

Amorphous and nanocrystalline anatase TiO_2 were prepared through a new route using peroxo-polytitanic acid (Ti-IPA). The capacity of anatase TiO_2 with average particle size of 25 nm prepared by heating the amorphous precursor at 300 °C for 5 h was 158 mAh/g at rather high rate 1.08 C. Elevating the heating temperature to 400 °C or 500 °C resulted in the reduction of the capacity. Heating at 300 °C is favorable for lithium insertion and deinsertion, because crystal growth and aggregation to form secondary particles are suppressed and lattice defects are diminished. We also presented a theoretical discussion on the relationship between energy distribution of insertion sites and discharge curves, and developed a numerical calculation method of the energy distribution of insertion sites from the discharge curves. The nanocrystalline anatase

TiO_2 showed uniform site energy distributions reflecting the homogeneous insertion sites, whereas the amorphous phase had a broad energy distribution reflecting the heterogeneous structure. The energy distribution curves calculated from the discharge curves will be very useful to discuss the insertion sites in crystal structures.

Acknowledgments

The authors are grateful to Prof. Tetsuichi Kudo for helpful advice and to Messrs. Kazuki Iwata and Kazuki Sakamoto for their assistance in the preliminary experiments of this work.

References

1. J. Wang, H. Zhao, Q. Yang, C. Wang, P. Lv, Q. Xia, *J. Power Sources*, **222**, 196 (2013).
2. V. Gentili, S. Brutti, L. J. Hardwick, A. R. Armstrong, S. Panero, P. G. Bruce, *Chem. Mater.*, **24**, 4468 (2012).
3. M. Wang, C. Li, W. Lai, S. Yen, *Thin Solid Films*, **520**, 6744 (2012).
4. M. Tsai, J. Chang, H. Sheu, H. Chiu, C. Lee, *Chem. Mater.*, **21**, 499 (2009).
5. M. Zukalova, M. Kalbac, L. Kavan, I. Exnar, M. Graetzel, *Chem. Mater.*, **17**, 1248 (2005).
6. H. Furukawa, M. Hibino, I. Honma, *J. Electrochem. Soc.*, **151**, A527 (2004).
7. L. D. Noailles, C. S. Johnson, J. T. Vaughey, M. M. Thackeray, *J. Power Sources*, **81**, 259 (1999).
8. Y. Yagi, M. Hibino, T. Kudo, *J. Electrochem. Soc.*, **144**, 4208 (1997).
9. D. Wang, D. Choi, Z. Yang, V. V. Viswanathan, Z. Nie, C. Wang, Y. Song, J. Zhang, J. Liu, *Chem. Mater.*, **20**, 3435 (2008).
10. I. Tsuyumoto, M. Kobayashi, T. Are, N. Yamazaki, *Chem. Mater.*, **22**, 3015 (2010).
11. F. Izumi, K. Momma, *Solid State Phenom.*, **130**, 15 (2007).
12. M. Wagemaker, W. J. H. Borghols, F. M. Mulder, *J. Am. Chem. Soc.*, **129**, 4323 (2007).
13. C. J. Howard, T. M. Sabine, F. Dickson, *Acta Cryst. B*, **47**, 462 (1991).
14. M. Okubo, E. Hosono, J. Kim, M. Enomoto, N. Kojima, T. Kudo, H. Zhou, I. Honma, *J. Am. Chem. Soc.*, **129**, 7444 (2007).